Accumulation of Microstructural Damage Due to Fatigue of High-Strength Aluminum Alloys

A. J. Luévano, M. A. Przystupa, and J. Zhang

The microstructural features of aluminum alloy 7050-T7451 in the vicinity of fatigue cracks and on the crack path were studied to determine which of these features influence fatigue crack propagation. The studies included characterization of the full spectrum of microstructural and fracture surface features—from the largest (e.g., roughness and grain type) to the smallest (e.g., second-phase particles and dislocations). Of all the features studied, only the second-phase particles were shown to have a definite influence by causing crack deflection. The number of particles encountered by the fatigue cracks were significantly higher than the expected average. The fatigue crack path was predominately transgranular, and there was no change in the dislocation and precipitation structures in the crack-affected zone.

Keywords

Aluminum alloys, cracks: propagation, fatigue

1. Introduction

FATIGUE failures in metals and alloys are always preceded by the accumulation of microstructural damage. Such damage manifests itself as microcracking, debonding, development of slip bands, formation of dislocation cell structures, and, ultimately, nucleation and growth of a fatigue crack. The sequence of damage accumulation events leading to the fatigue crack nucleation and growth is debatable, but there is no doubt that fatigue resistance is low in alloys susceptible to large amounts of microstructural damage (Ref 1). In order to design alloys for improved fatigue resistance and/or to formulate realistic life-prediction models, it is thus necessary to determine which forms of damage occur in different alloys and to rank their importance.

The purpose of this work was to identify microstructural damage processes taking place during fatigue in a typical precipitation-hardened aluminum aerospace plate alloy and to assess the importance of these processes in controlling crack propagation rates. Aluminum alloys were chosen because of their prominence in aerospace applications. These alloys also have very complex structures consisting of unrecrystallized or partially recrystallized grains with matrix and grain-boundary precipitates, constituent particles, microporosities, and, in many instances, precipitation-free zones (Ref 2-5). The dominant fatigue crack usually initiates at the largest surface micropore and propagates tortuously through the matrix. Crack deflections results from the linking up of the main crack with microcracks in the damage zone preceding it or from preferred intergranular fracture, cracking along slip planes, and so on. Each of these factors constitutes a different type of microstructural damage mechanism. The mechanism that is actually active can be identified through metallographic and fractographic examinations. The results of such an analysis, for the 7050-T7451 plate alloy, are reported here. Included is information about the crack geometry, the distribution of different features on the crack path, and the microstructural damage inflicted during fatigue.

A.J. Luévano, M.A. Przystupa, and **J. Zhang,** Department of Materials Science and Engineering, University of California, Los Angeles, Los Angeles, CA 90024

2. Experimental Procedure

The material used in this study was from the center of a batch of 14.5 cm thick 7050-T7451 plate alloy designated as "old quality" by Alcoa. This alloy (Fig. 1) is 20% recrystallized and contains, by volume, about 0.1% of porosities and 0.65% constituent particles in the form of stringers (Ref 6). Their average sizes are 3.4 and 4.5 μm, respectively (Ref 6). The precipitate microstructure consists of grain-boundary and matrix precipitates (Fig. 2).

The precipitate phases present were identified by comparing the diffraction patterns of the examined alloy with patterns of other 7*xxx* alloys. The patterns were identical to those taken by Park and Andrell (Ref 7) of overaged 7075. They identified the matrix phases as η′ and η variants (predominantly η1, η2, and η4) and the grain-boundary precipitates as predominantly η. Because the alloy had been partially recrystallized, the dislocations were not apparent in these microstructures.

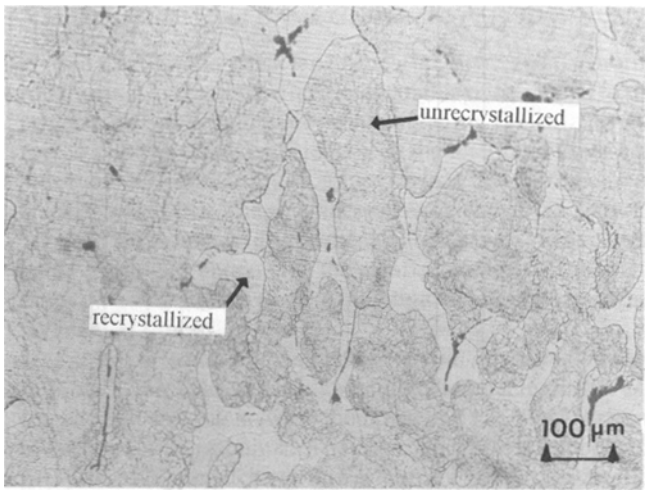

Fig. 1 Micrograph showing recrystallized and unrecrystallized grains in aluminum alloy 7050-T7451

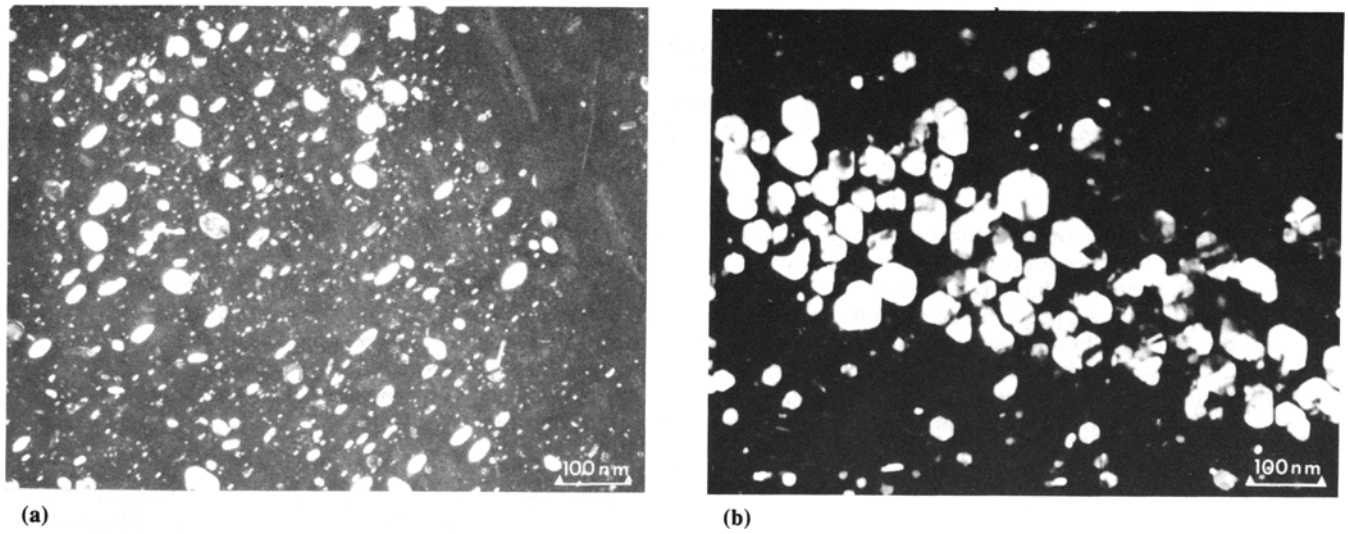

Fig. 2 Microstructure of 7050-T7451 grain-boundary precipitates (a) and matrix precipitates (b)

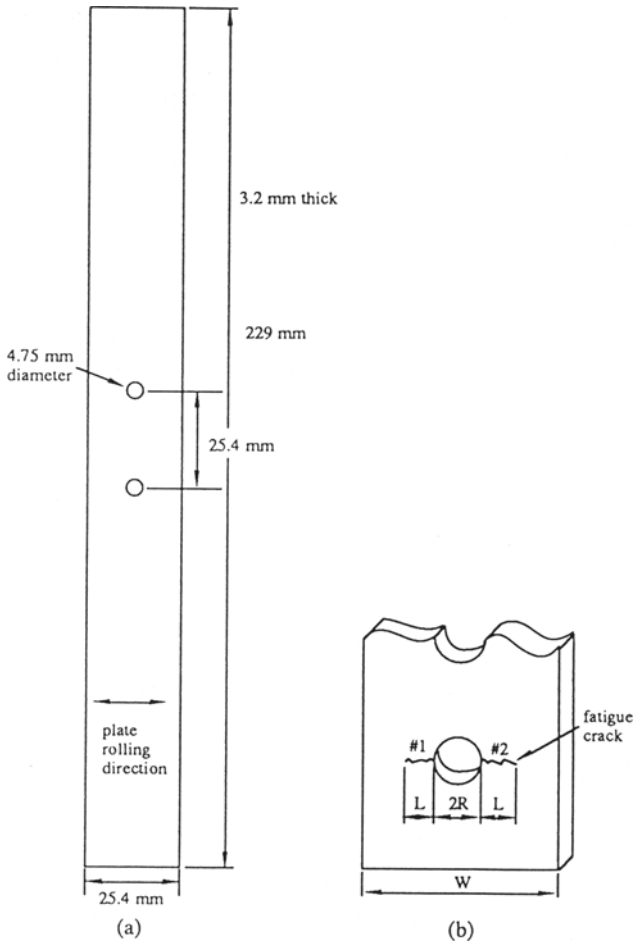

Fig. 3 (a) Two-hole fatigue sample. (b) Schematic of secondary fatigue cracks

The samples for damage assessment used in this investigation were cut from two-hole fatigue specimens (Fig. 3a). Two-hole specimens were used to simulate the loading condition of bolt holes in an aircraft part (Ref 3-5). The specimens were cut from the center section of a plate, with the long axis normal to the rolling direction. They were then fatigued to failure under the conditions of $\sigma_{max} = 170$ MPa, $R = 0.1$, and a frequency of 10 Hz. In all cases, the cracking started from large surface micropores (Ref 5). Some of the failed samples contained secondary fatigue cracks at the unfailed hole (Fig. 3b). These cracks are ideal for identifying the microstructural features on both sides of the fatigue crack path. The microstructures in the vicinity of two such cracks that formed on opposite sides of the same hole were studied in this investigation, which employed both scanning electron microscopy (SEM) and transmission electron microscopy (TEM).

The SEM examinations were used to determine the crack roughness, the relationship of the crack path to grain structure, the number of second-phase particle intercepts, and the severity of microcracking. The microstructures were characterized along two crack paths (Fig. 3b) at the surface sections and at the one-third and two-thirds thicknesses of the sample. Scanning electron microscopy photographs of specimens in both the etched and unetched conditions were used for all measurements. Actual crack lengths and the fractions of the crack paths through various regions (i.e., unrecrystallized grains, recrystallized grains, and grain boundaries) were measured on the micrographs using a digitizer.

One of the cracks was analyzed using a computerized system for fractographic analysis (Ref 8). This system allows automatic estimation of the actual and projected crack lengths, roughness parameters, distribution of the angles describing orientations of crack segments, and fractal dimension. The general concept of the fractal analysis is based on the principle that the number of ruler lengths, N, required to measure the length

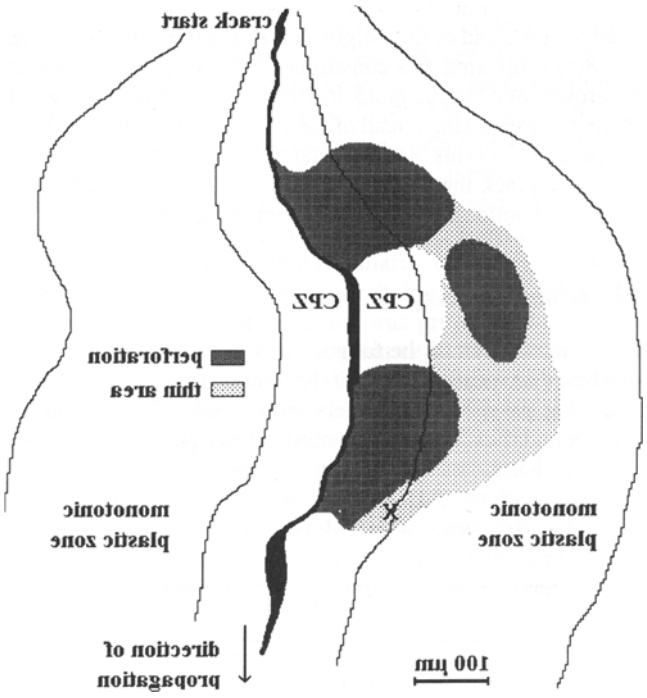

Fig. 4 Schematic of thin foil used for dislocation study. The thinned area examined is marked with an X

of a curve depends on the size of the ruler, ρ, used in the measurement (Ref 9). A small ruler resolves finer details than a large one, but at the same time requires a disproportionately greater number of steps to cover the analyzed curve. A plot of log (N) versus log (1/ρ) for a fractal curve yields a straight line that can be described by:

$$N = k\left(\frac{1}{\rho}\right)^{d}$$

where d is the fractal dimension and k is a constant. Such a defined fractal dimension gives an indication of the roughness of a surface: The closer the number is to 1, the smoother the surface. This method of defining a fractal has been proposed by Mandelbrot (Ref 9).

To determine whether a fatigue crack deflects toward constituent particles, the average number of particles per unit length of a straight line was compared with the actual number of particles per unit crack length. For both measurements, enlarged photographs of the entire crack length were used. The expected number of particles for a straight crack was measured using a scan grid of parallel lines spaced 0.5 cm apart. Because of the anisotropy of constituent particle spatial distribution, the grid was always aligned with the average direction of crack propagation. The number of constituent particle intercepts per unit length along the actual crack path was calculated from measurements of the actual crack lengths and total number of particles intersected by the crack.

Table 1 Crack lengths and roughness parameters

Crack No.	Section	Projected length, μm	Actual length, μm	Profile roughness parameter
1	Surface	1937	2400	1.24
	1/3 thickness	2771	3277	1.18
	2/3 thickness	2773	3307	1.19
2	Surface	3292	3635	1.10
	1/3 thickness	3600	4037	1.12
	2/3 thickness	3433	4171	1.22

The SEM studies were supplemented by TEM examination to determine whether any change in dislocation structure occurred in the vicinity of the crack path. Specifically, evidence of dislocation activities in or near the cyclic plastic zone was sought. Samples for this purpose were cut from various sections along the fatigue crack path. Each TEM sample contained either starting, middle, or end regions of the fatigue crack. The samples were dimpled using a solution of 10% nitric acid and 90% water at room temperature and a voltage of 25 V. Final polish and perforation were done with a solution of 30% nitric acid and 70% methanol at a temperature of –30 °C and a voltage of 15 to 18 V.

All TEM samples were examined in the scanning (STEM) mode to determine the position of the perforations in relation to the fatigue crack. The thinned area around the perforation chosen for examination was always the one closest to the crack. Because little control over the position of the perforation is possible, we were unsuccessful in obtaining samples with suitable thinned area next to the crack. The location of the thinned area closest to the fatigue crack used in this study is shown schematically in Fig. 4. As indicated in Fig. 4 and explained in the following section, this area was on the border between the cyclic and the monotonic plastic zones. All other TEM samples were from the monotonic plastic zone.

3. Results and Discussion

3.1 *Roughness and Crack Geometry*

The results of the crack length measurements and the profile roughness parameters, defined as the ratios of the actual to the projected crack lengths, are summarized in Table 1. As expected, the projected crack lengths in the interiors of the samples were longer than those at the surface due to the curved crack front profile. The roughness parameters varied between 1.1 and 1.24, which is in agreement with the average roughness parameter of 1.2 obtained in the parallel studies for the actual fatigue fracture surfaces of the investigated sample using fractal analysis (Ref 6).

Profiles of crack 2 at the surface section opposite that used in Table 1 were analyzed using an automated fractographic and fractal analysis system. Both the upper and the lower surfaces of the crack were examined. The crack length for the upper profile was 3128 μm; for the lower surface profile, 3028 μm. Roughness parameters were 1.27 and 1.25, respectively (a difference of only 1.35%). Results of the fractal analysis for the upper surface profile of crack 2 are shown in Fig. 5. The slopes

of the curve is 1.041, which represents the fractal dimension. The fractal dimension for the lower profile was a comparable 1.037. The results indicated only one of the profiles required study.

The distribution of the crack segment orientations for the upper profile of crack 2 is shown in Fig. 6. As expected, the most frequent angle for the upper profile is at about 90°, which is the general crack propagation direction. The lower profile exhibited a similar symmetrical trend. Both distributions were relatively flat, indicating a considerable amount of crack deflection in both profiles.

In addition to the main fatigue cracks, two other types of cracks were observed in the studied specimens. The more common type was crack branching. The branches often grew toward and into constituent particles (Fig. 7a). Microcracks were also observed near, but separate from, the main crack. Two examples of such microcracks are shown in Fig. 8. Both were located near the end of the fatigue crack, and the crack shown in Fig. 8(a) originated at a constituent particle. This means that the growth of a fatigue crack in 7050-T7451 alloy is preceded by the microcracking ahead of the crack tip, with the constituent particles serving as the potential microcrack nucleation sites. The crack then propagates toward the microcracks, resulting in a noticeable amount of crack deflection.

3.2 *Grain Structure*

The interaction of the fatigue crack with grains was evaluated based on measurements of the fractions of the length of the crack that passed through the various types of grains and/or grain boundaries. Because the material was partially recrystal-

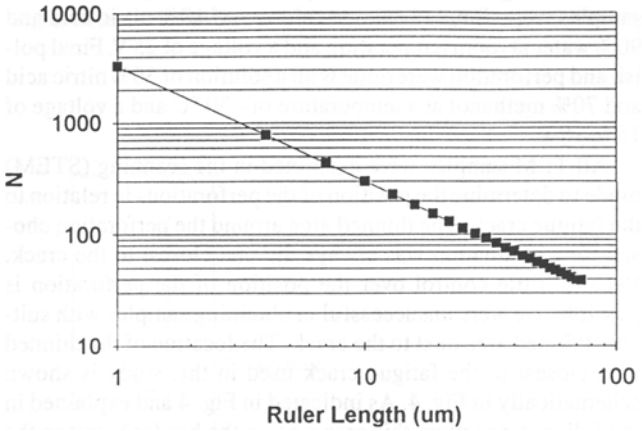

Fig. 5 Plot for determining fractal dimensions of fatigue crack 2, upper profile, surface region

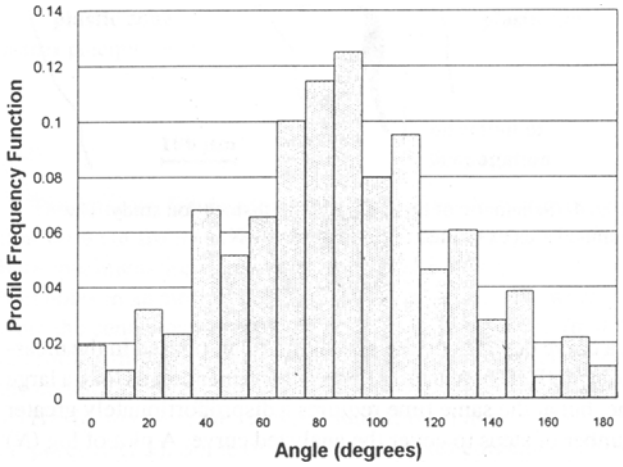

Fig. 6 Distribution of angular orientation of crack segment, crack 2, surface section

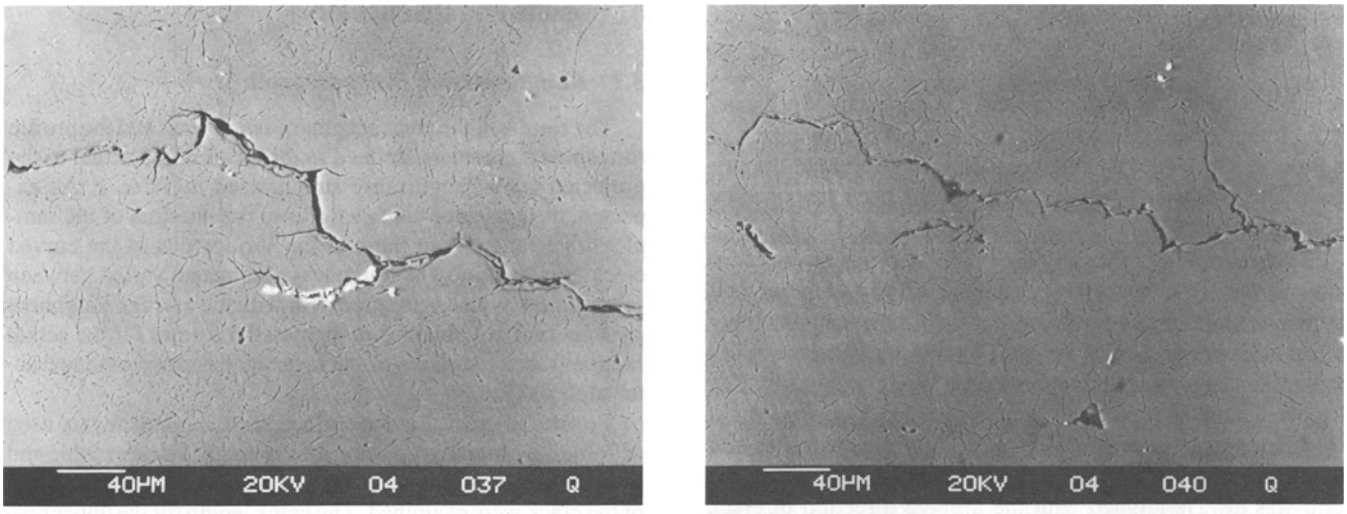

(a) (b)

Fig. 7 Branching of fatigue cracks in 7050-T7451 alloy. (a) Branches propagating through constituent particles. (b) Branches propagating along grain boundaries

lized, the grains encountered by the crack were either recrystallized or unrecrystallized with subgrains. The lengths of the crack path along boundaries and through each type of grains were measured from micrographs and used in the calculation of the percentages. Intergranular portions of the crack path were separated into the following categories, depending on the types of grains on either side of the crack: (1) unrecrystallized/recrystallized, (2) recrystallized/recrystallized, and (3) unrecrystallized/unrecrystallized. The results (Table 2) indicate that the crack propagated both transgranularly and intergranularly, with the preferred fracture mode being transgranular. The transgranular portion of the crack was primarily through the unrecrystallized grains which is not unexpected as the material is only 20% recrystallized. The fractions of the recrystallized grains encountered by the crack varied widely, but generally were lower than the recrystallization levels.

Intergranular failures constituted between 6 and 40% of the total fatigue crack path. From the possible combinations, the boundaries between unrecrystallized and recrystallized grains were most frequently chosen by the crack. This implies that such boundaries are most susceptible to fatigue damage. It was also observed that some of the transgranular cracks in the unrecrystallized grains propagated along subgrain boundaries. The percentages of crack path along subgrain boundaries in the unrecrystallized grains, also given in Table 2, indicate that only a small portion of the crack path followed subgrain boundaries. In the case of crack 2, the crack was too wide to allow accurate determination of its path.

3.3 *Second-Phase Particles*

To determine the influence of the constituent particles on the crack path deflections, the expected number of particle intercepts along a straight line through a sample were compared with the number of particles intercepted by the actual crack path. As described earlier, the measurements were taken from enlarged photographs (e.g., Fig. 9) that enhanced the details. The results are summarized in Table 3. For each section the number of particle intercepted by the crack was always greater than the expected average for the straight line. To determine whether the values were significantly different, the null hypothesis that they were the same was tested using Student's t-distribution (Ref 10). In all cases the null hypothesis

Table 2 Percentage of crack length in various regions of grain structure

Sample		Transgranular crack path			Intergranular crack path (a)				
		Unrecrystallized,	Recrystallized,	Total,	U/R boundaries,	R/R boundaries,	U/U boundaries,	Subgrain,	Total,
Crack No.	Section	%	%	%	%	%	%	%	%
1	Front surface	76.1	12.3	88.4	2.2	1.5	...	7.9	11.6
	1/3 thickness	54.3	5.9	60.2	25.8	7.2	5.1	1.7	39.8
	2/3 thickness	63.4	22.4	85.8	12.6	...	1.5	...	14.2
	Back surface	65.6	12.8	78.4	12.8	8.8	...	...	21.6
2	Surface	65.8	26.2	92.0	8.0	...	...	...	8.0
	1/3 thickness	75.7	18.5	94.2	5.8	...	...	...	5.8

(a) U/R, unrecrystallized/recrystallized; R/R, recrystallized/recrystallized; U/U, unrecrystallized/unrecrystallized

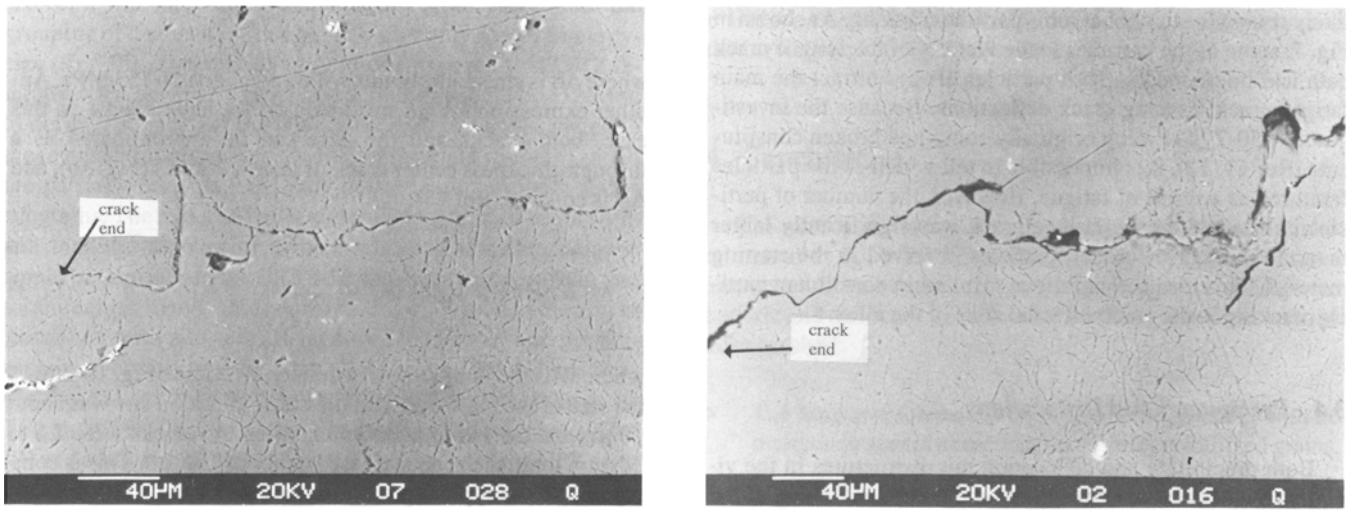

(a) (b)

Fig. 8 Microcracks in the vicinity of the main crack. Arrows indicate the end of the fatigue crack.

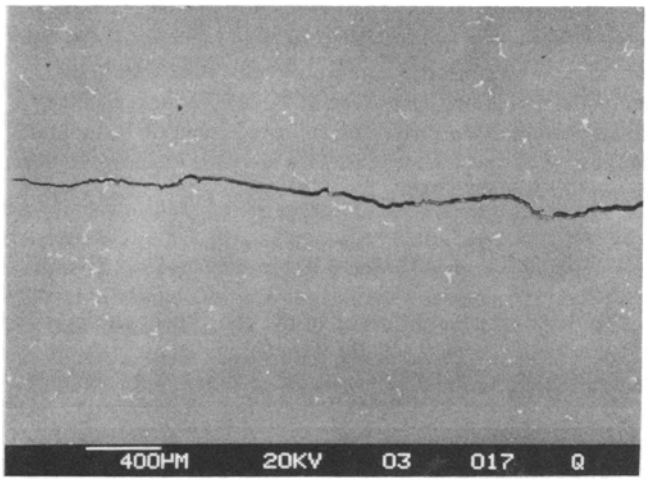

Fig. 9 Example of the type of micrograph used to calculate the number of particles intercepted by scan lines and the crack

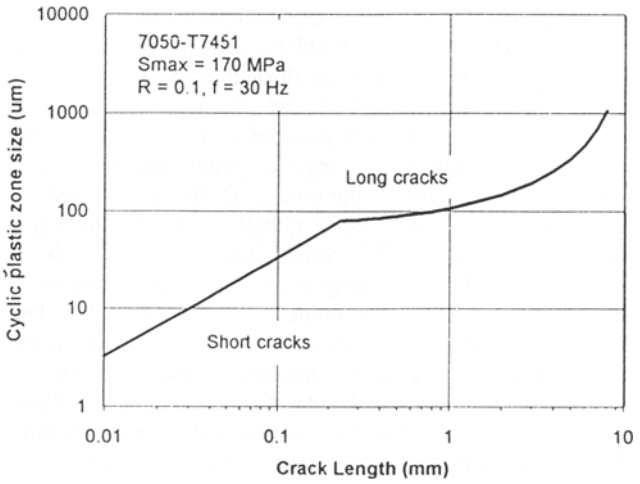

Fig. 10 Changes in CPZ size with crack length

Table 3 Number of intercepts of scan lines and crack path with second phase particles.

Crack No.	Section	Straight line No./μm	Crack path No./μm	Significance level (%)
1	surface	$9.9 \times 10^{-4} + 6.5 \times 10^{-4}$	2.0×10^{-3}	<0.1
	1/3 thickness	$8.7 \times 10^{-4} + 4.5 \times 10^{-4}$	2.1×10^{-3}	<0.1
	2/3 thickness	$9.4 \times 10^{-4} + 5.8 \times 10^{-4}$	1.6×10^{-3}	<0.1
2	surface	$8.0 \times 10^{-4} + 5.8 \times 10^{-4}$	1.3×10^{-3}	<0.1
	1/3 thickness	$1.2 \times 10^{-4} + 5.8 \times 10^{-4}$	1.9×10^{-3}	<0.1
	2/3 thickness	$1.0 \times 10^{-3} + 4.1 \times 10^{-4}$	2.2×10^{-3}	<0.1

had to be rejected at a significance level of less than 0.1%. This means that there was a less than 0.1% chance that the number of particles intercepted by the crack was the same as that for the straight line; the actual calculated probability was even smaller (in the 1×10^{-10}% range).

It is thus justifiable to conclude that the constituent particles affected the crack path by causing crack deflections. The most likely reason for this behavior is particle cracking. As shown in Fig. 7, some of the particles in the vicinity of the fatigue crack path had microcracks. Such particles always attract the main fatigue crack, causing crack deflections. Because the investigated 7050-T7451 alloy originally contained broken constituents (Ref 11, 12), it is impossible to tell which of the particles fractured as a result of fatigue. However, the number of particles intersected by the fatigue crack was significantly larger than the number of broken particles observed in the starting material. This means that fatigue resulted in constituent particle cracking in the crack-affected zone of the alloy.

3.4 *Precipitates and Dislocations*

Both precipitate and dislocation microstructures in the vicinity of the crack were examined and compared to that of the bulk material to establish whether fatigue-related damage occurred. Because the studied material was subjected to high-cycle fatigue, the most probable region of damage was the cyclic plastic zone (CPZ). To determine the size of that zone and thus how close to the fatigue crack the TEM sample had to be perforated, Eq 1 was used (Ref 1):

$$r_c = \frac{1}{\pi}\left(\frac{\Delta K}{2\sigma_y}\right)^2 \qquad \text{(Eq 1)}$$

where ΔK is the stress-intensity factor amplitude and σ_y is the yield strength, equal to 450 MPa for 7050-T7451 alloy.

The change in the CPZ size, r_c, with crack length using Eq 1 is shown in Fig. 10. Two cases had to be considered. The first involved small through-thickness cracks, each of length L, emanating from the fasten hole of radius R. In this case, the stress-intensity factor can be approximated as (Ref 13, 14):

$$\Delta K = 3.36\Delta\sigma\sqrt{\pi L}\sqrt{\frac{2R + 2L}{2R + L}} \qquad \text{(Eq 2)}$$

where $\Delta\sigma$ is stress amplitude, which was equal to 153 MPa. Another expression for ΔK must be used for large cracks. In this case, both cracks and the hole can be approximated as a through-thickness center crack of length $2(R+L)$ (Fig. 3b), and ΔK is equal to (Ref 13):

$$\Delta K = \Delta\sigma\sqrt{\pi(R + L)}\left(\sec\frac{\pi(R + L)}{W}\right)^{1/2} \qquad \text{(Eq 3)}$$

where W is the double-hole specimen width. As Fig. 10 shows, the size of the plastic zone at the crack initiation site was about 10 μm. At the termination point, when the cracks were 2.5 to 3.5 mm long, the zone increased to about 250 μm. This is comparable to the typical grain size, which for the studied 7050-T7451 alloy is 138 μm for unrecrystallized grains. Thus, to observe any possible damage due to fatigue, the TEM sample had to be perforated in a grain adjacent to the fatigue crack. Such accuracy is difficult to achieve. However, as shown in Fig.

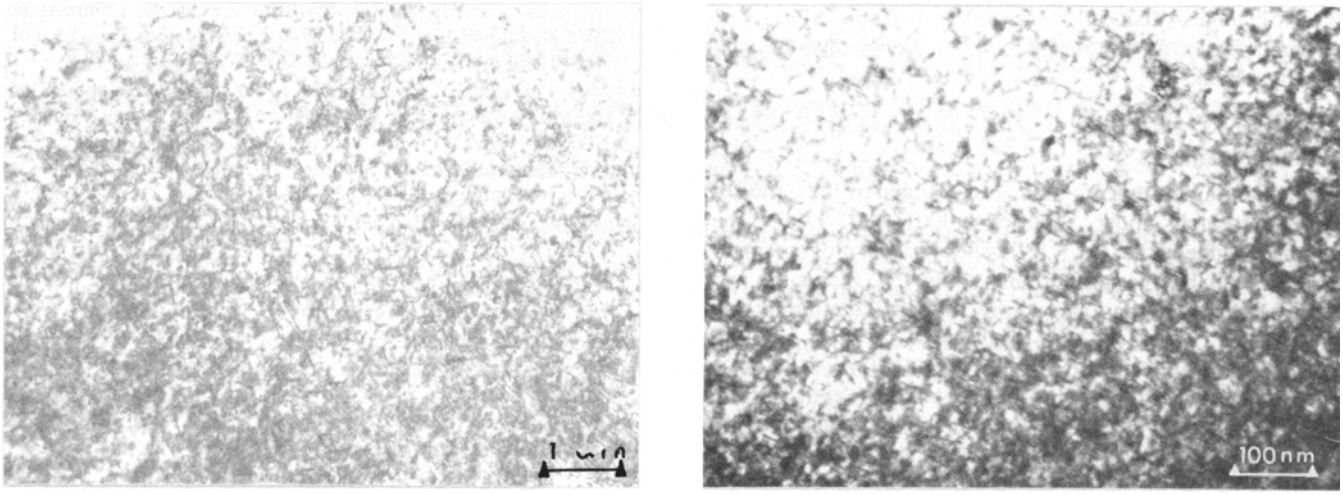

(a) (b)

Fig. 11 Microstructure of the matrix in (a) bulk 7050-T7451 and (b) thin foil closest to the crack shown

4, we were able to obtain a foil with perforation approximately 0.7 mm from the crack initiation site and 100 μm from the crack surface. The CPZ in this area was about 100 μm (Fig. 10). Hence, the area examined was not in the CPZ, but on the border between the CPZ and the monotonic plastic zone. Examination of that particular sample revealed no evidence of changes in the precipitate structure or debonding at the grain boundaries. Also, the dislocation structure was no different from that of the bulk material. Figure 11 compares the microstructure of the matrix in the bulk 7050-T7451 material and in the area indicated in Fig. 4. Although the dislocations are difficult to locate, there clearly are no tendencies to grouping and/or banding in the area nearest the CPZ.

The above findings are consistent with other studies of dislocation structure in 7*xxx* alloys in low-cycle fatigue. For instance, it was reported that even at low strain amplitudes the grouping of dislocations can be seen after only a few fatigue cycles (Ref 16). The studied sample was exposed to 47,812 fatigue cycles, so some dislocation activities should be expected to occur. The fact that none was observed can be attributed to the low maximum stress (only 38% of the yield strength) and to the partially recrystallized polygonized structure with stable subgrains. The material had few free dislocations to begin with, and thus the amount of fatigue-related dislocation damage would be confined to the CPZ and would be much less than that for unrecrystallized, cold-worked alloys. Moreover, the slip in 7*xxx* aluminum alloys is affected by both temper and the percentage of copper present in the alloy. In the T7 stabilized temper, these alloys have more unshearable precipitates than in the T6 condition. Therefore, the slip is more homogeneous (Ref 17) and crack-tip deformation can be absorbed in the CPZ area. The affect of aging on the dislocation structure of 7050 alloy fatigued under low- cycle, low-strain-amplitude conditions was investigated by Coyne and Starke (Ref 18). They reported that going from underaged to peak aged to overaged conditions resulted in decreased dislocation banding and lower dislocation densities within the bands. The effect of copper on slip is similar. As the copper content increases, slip becomes more homogeneous and slip bands are not observed. Lin and Starke (Ref 19), observed this phenomenon in 7*xxx* alloys with 2.1% Cu. Our alloy contained 2.3% Cu. and was in the overaged condition. The lack of dislocation activities is consistent with the Lin and Starke findings. However, some dislocation activities had to have taken place to facilitate fracture. The fact that none was observed can be explained by the location of the TEM examination areas. All areas examined were on the border outside the CPZ and thus in the region where plastic deformation would be small. As reported by Wilkins and Smith (Ref 20), moving away from the crack tip from the cyclic to the monotonic plastic zone, the dislocation structure changes from one characteristic of high-strain fatigue to one of low-strain fatigue. Results of our study confirm this and indicate that no visible dislocation activities occurred in the monotonic plastic zone in the investigated 7050-T7451 alloy.

4. Conclusions

The microstructure in and adjacent to fatigue cracks in aluminum alloy 7050-T7451 has been characterized to assess the amount of fatigue damage on the grain structure, second-phase particle and dislocation levels. The following conclusions have been reached:

- The fatigue crack path is 60 to 95% transgranular, with no preference toward unrecrystallized or recrystallized grains.
- The intergranular portion of the crack path occurs preferentially between unrecrystallized and recrystallized grains.
- Deflection of crack paths is controlled by the second-phase particles. The number of particles on the crack path is significantly higher than the expected average.

- No change in dislocation structure and no alterations of the precipitate structure was observed in the vicinity of the fatigue cracks.

Acknowledgements

The funding for this program was provided by the Office of Naval Research under contract N00014-91-J-1299. The authors are indebted to Dr. A.K. Vasudévan, the program manager, for valuable discussions and to Drs. P.E. Magnusen and R.J. Bucci from Alcoa Laboratories for providing the fatigue samples.

References

1. S. Suresh, *Fatigue of Materials*, Cambridge University Press, 1991
2. A.K. Vasudévan, R.D. Doherty, and S. Suresh, Fracture and Fatigue Characteristics in Aluminum Alloys, *Aluminum Alloys—Contemporary Research and Applications, Treatise on Materials Science and Technology*, Vol 31, A.K. Vasudévan and R.D. Doherty, Ed., Academic Press, 1989, p 446
3. C.R. Owen, R.J. Bucci, and R.J. Kegarise, Aluminum Quality Breakthrough for Aircraft Structural Reliablility, *J. Aircraft*, Vol 26, 1989, p 178-184
4. A.J. Hinkle, P.E. Magnusen, R.L. Rolf, and R.J. Bucci, Effect of Microporosity on Notched Specimen Fatigue Life, *Proceedings. of 5th International Conference on Structure Safety and Reliability*, A. H-S. Ang., M. Shinozuka, and G.I. Schueller, Ed., American Society of Civil Engineers, 1989, p 1467-1474
5. J.R. Brockenbrough, R.J. Bucci, A.J. Hinkle, J. Liu, P.E. Magnusen, and S.M. Miyasato, "Role of Microstructure on Fatigue Durability of Aluminum Aircraft Alloys," F33615-92-C-5915, Alcoa, 1993
6. M.A. Przystupa, J. Zhang, and A.J. Luévano, "Development of the Microstructure Based Stochastic Life Prediction Models," N00014-91-J-1299, University of California Los Angeles, 1992—(available from Defense Technical Information Center, Bldg. 5, Cameron Station, Alexandria, VA 22304-6145)
7. J.K. Park and A.J. Ardell, Microstructures of the Commercial 7075 Al Alloy in the T651 and T7 Tempers, *Metall. Trans. A*, Vol 14A, 1983, p 1957-1965
8. M.A. Przystupa, J. Zhang, and A.J. Luévano, "Development of the Microstructure Based Stochastic Life Prediction Models," N00014-J-1299, University of California—Los Angeles, 1993 (available from Defense Technical Information Center, Buld. 5, Cameron Station, Alexandria, VA 22304-6145).
9. B.B. Mandelbrot: *Fractal Geometry of Nature*, W.H. Freeman, 1982.
10. E.L. Crow, F.A. Davis, and M.W. Maxfield, in *Statistical Manual*, Dover Publications, 1960, p 37
11. M.A. Przystupa, J. Zhang, and A.J. Luévano, "Development of the Microstructure Based Stochastic Life Prediction Models," N00014-J-1299, University of California—Los Angeles, 1991 (available from Defense Technical Information Center, Buld. 5, Cameron Station, Alexandria, VA 22304-6145).
12. J. Zhang, A.J. Luévano, and M.A. Przystupa, Quantitative Analysis of Heterogeneous Grain Structure on Plane Sections, *Scr. Metall. Mater.*, Vol 26, 1992, p 1061-1066
13. R.C. Shah, Stress Intensity Factors for Through and Part-Through Cracks Originating at Fastener Holes, in *Mechanics of Crack Growth*, STP 590, ASTM, 1976, p 429-459
14. O.L. Bowie, *J. Math. Phys.*, Vol 35, 1956, p 60-71
15. D. Broek, in *Elementary Engineering Fracture Mechanics*, 4th ed., Kluwer Academic Publishers, 1991, p 85
16. C. Laird, Mechanisms and Theories of Fatigue, in *Fatigue and Microstructure*, American Society for Metals, 1978, p 149-204
17. F.-S. Lin and E.A. Starke, Jr., The Effect of Copper Content and Deformation Mode of the Fatigue Crack Propogation of Al-6Zn-2Mg-xCu Alloys at Low Stress Intensities, *Mater. Sci. Eng.*, Vol 45, 1980, p 153-165
18. E.J. Coyne, Jr. and E.A. Starke, Jr., The Effect of Microstructure on the Fatigue Crack Growth Behaviour of an Al-Zn-Mg-(Zr) Alloy, *Int. J. Fract.*, Vol 15(No. 5), 1979, p 405-417
19. F.-S. Lin and E.A. Starke, Jr., The Effect of Copper Content and Degree of Recrystallization on the Fatigue Resistance of 7XXX-type Aluminum Alloy, *Mater. Sci. Eng.*, Vol 43, 1980, p 65-76
20. M.A. Wilkins and G.C. Smith, Dislocation Structures Near a Propagating Crack in an Al//2% Mg Alloy, *Acta Metall.*, Vol 18, 1970, p 1035-1043